JOURNAL OF GEOPHYSICAL RESEARCH, VOL. 86, NO. C9, PAGES 8107–8116, SEPTEMBER 20, 1981

Modeling of Anisotropic Electromagnetic Reflection From Sea Ice

K. M. GOLDEN AND S. F. ACKLEY

U.S. Army Cold Regions Research and Engineering Laboratory, Hanover, New Hampshire 03755

The contribution of brine layers to observed reflective anisotropy of sea ice at 100 MHz is quantitatively assessed, and a theoretical explanation for observed reflective anisotropy is proposed in terms of anisotropic electric flux penetration into the brine layers. The sea ice is assumed to be a stratified dielectric consisting of pure ice containing ellipsoidal conducting inclusions (brine layers) uniformly aligned with their long axes perpendicular to the preferred crystallographic c axis direction. The asymmetrical geometry of the brine layers is shown to produce an anisotropy in the complex dielectric constant of sea ice. The contribution of these layers to the reflective anisotropy is examined with a numerical method of approximating the reflected power of a radar pulse incident on a slab of sea ice. Mixture dielectric permittivities are calculated for both the electric fields parallel and perpendicular to the c axis direction. These permittivities are then used to calculate power reflection coefficients at each interface in the air/sea ice/sea water system. Significant bottom reflection ($R \approx 0.09$) occurs when the polarization is parallel to the c axis. However, when the polarization is perpendicular to the c axis, the return is almost completely extinguished ($R < 0.003$). This extinction is due primarily to absorptive loss associated with the conducting inclusions and secondarily to an impedance match at the ice/water interface that results in transmission rather than reflection of the wave.

1. INTRODUCTION

Recent studies of arctic fast ice [*Cherepanov,* 1971; *Weeks and Gow,* 1979; *Kovacs and Morey,* 1978] have shown that the crystallographic c axes (optic axes) of sea ice have not only a preferred horizontal orientation, but also a preferred azimuthal direction within the horizontal plane. *Campbell and Orange* [1974] and *Kovacs and Morey* [1978] have established that the strength of the return from impulse radar soundings (center frequency at 100 MHz) of sea ice depends strongly on direction. Maximum reflection from the ice/water interface occurs when the pulse is polarized so that the electric field parallels the preferred c axis direction. Minimum bottom reflection occurs when the polarization is perpendicular to the preferred c axis direction. In the most extreme cases of this anisotropy, the bottom signal appears to be almost completely extinguished (Figure 1).

Associated with a preferred c axis orientation within the horizontal plane is anisotropic brine structure. The ice/water interface where sea ice growth takes place consists of dendritic plates that are elongated perpendicular to the c axis direction and extend into the sea water below (Figure 2). As growth occurs, the sea water between the dendritic plates becomes trapped and makes up the so-called brine layers of sea ice [*Weeks and Assur,* 1967]. The brine layers near the sea ice bottom are elongated in the plane perpendicular to the c axis direction and have their shortest dimension parallel to the c axis direction. Thus maximum bottom reflection occurs when the electric field is normal to the principal brine/ice interface (normal polarization), and minimum bottom reflection occurs when the electric field is tangential to the principal brine/ice interface (tangential polarization).

An initial impetus for the present research was our dissatisfaction with the model proposed by *Kovacs and Morey* [1978] to explain the reflective anisotropy. In this model, the brine structure near the bottom of the ice is assumed to behave as a parallel plate waveguide, where 100 MHz is well below the cutoff frequency for parallel polarization in the guide. A fundamental problem with this theory is the lack of evidence for the existence of brine cells in parallel arrays of plates. We feel that it is more natural and predictively fruitful to consider the brine structure as consisting of individual, finite, anisotropic bodies rather than continuous plates (Figure 3).

2. THEORY

We propose that the asymmetrical geometry of the brine inclusions causes an anisotropy in the penetration of the impinging electric field into the brine layers. This anisotropic penetration is associated with an anisotropy in the effective complex dielectric constant of the sea ice, which determines the power returned to the receiver.

To facilitate analysis of the anisotropy, we assume that a slab of sea ice of thickness T is composed of l horizontal layers of uniform thickness d, which we take as 10 cm. Each layer i consists of pure ice of complex dielectric constant $\varepsilon_1 = \varepsilon_1' + j\varepsilon_1'' = 3.17 + j\,0.013$ [*Johari and Charette,* 1975] which surrounds uniformly distributed and aligned ellipsoidal brine inclusions of complex dielectric constant $\varepsilon_2 = \varepsilon_2' + j\varepsilon_2'' = 80 + j\,1000$ [*Vant,* 1976] and relative volume $v_b(i)$, where $j = \sqrt{-1}$. The geometry of the inclusions in layer i is specified by the principal axes $a(i)$, $b(i)$, and $c(i)$, and is characterized by the depolarization factors $n_k(i)$ defined by

$$n_k = \frac{abc}{2} \int_0^\infty \frac{ds}{(k^2 + s)\sqrt{(a^2 + s)(b^2 + s)(c^2 + s)}} \qquad (1)$$

where $k = a, b, c$ [*Stratton,* 1941]. These factors depend only on the axial ratios of the ellipsoids. The a axis of an ellipsoid is horizontal and perpendicular to the preferred crystal c axis direction, the b axis parallels this direction, and the ellipsoidal c axis is vertical, with $a > c \gg b$ near the sea ice bottom. The sea ice lies above a homogeneous half-space of sea water of complex dielectric constant $\varepsilon_w = 80 + j\,773$ [*Stratton,* 1941], and below a homogeneous half-space of air of complex dielectric constant $\varepsilon_A = 1 + j0$.

We will now examine the dielectric behavior of brine layers

Paper number 1C0767.

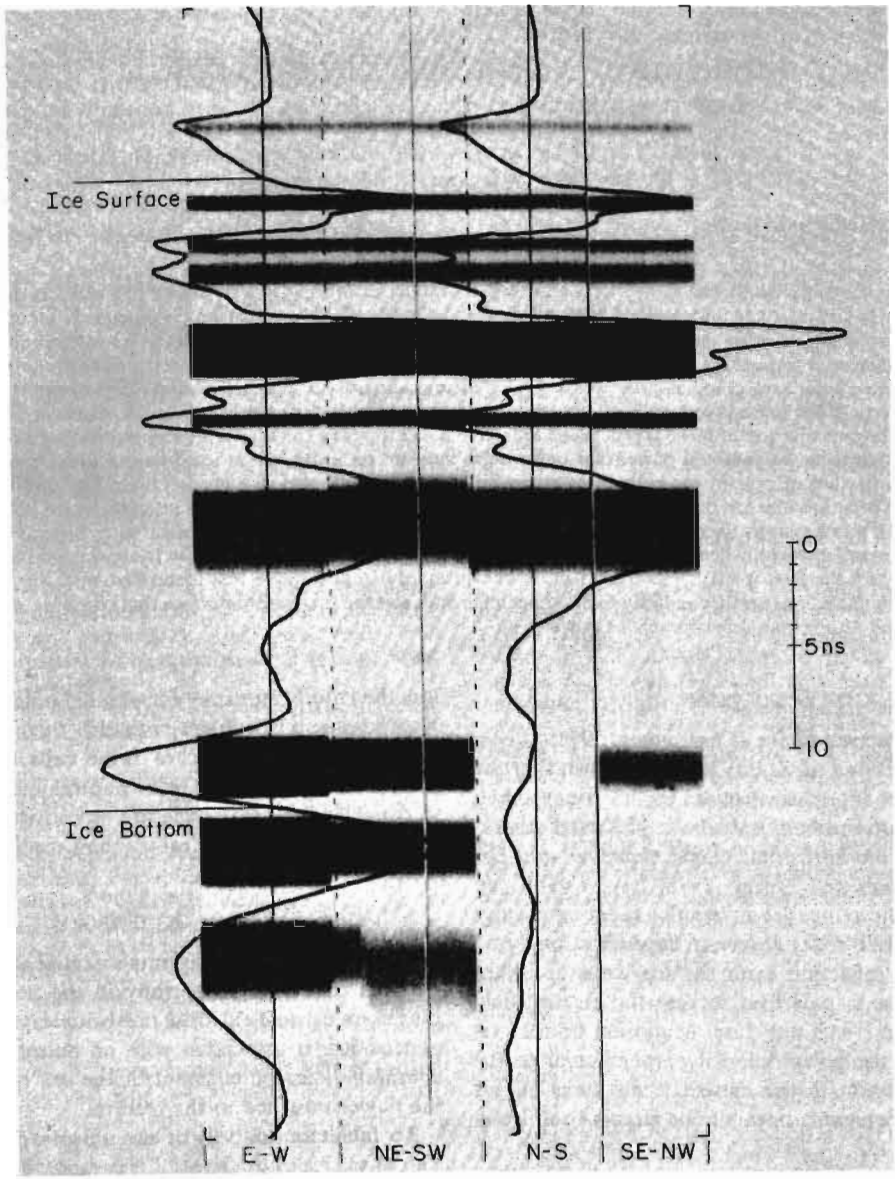

Fig. 1. Maximum and minimum bottom reflections spaced at 90° [from *Kovacs and Morey*, 1978].

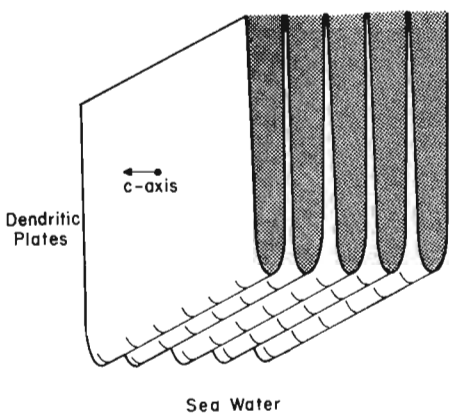

Fig. 2. Dendritic plates at ice/water interface, elongated perpendicular to the *c* axis direction, extending into the sea water below. Sea water trapped between the plates becomes the brine layers [from *Weeks and Gow*, 1979].

to understand the observed reflective anisotropy. We will examine the behavior of the radar pulse by only considering dielectric and reflective properties of the center frequency of the plane wave pulse.

Anisotropic Electric Flux Penetration

The electric field E_{2k} inside one of the ellipsoidal inclusions in the bottom layer l, when subjected to an initially uniform electric field E directed along one of the principal axes $k = a, b, c$, is given by [*Tinga et al.*, 1973]

$$E_{2k} = \frac{1}{\varepsilon_1 + n_k(l)(1 - \nu_b(l))(\varepsilon_2 - \varepsilon_1)} E \qquad (2)$$

and is independent of position inside the ellipsoid. This positional independence depends primarily on the condition that $a \ll \lambda$, which is satisfied for the wavelength $\lambda = 1.7$ m at 100 MHz in pure ice.

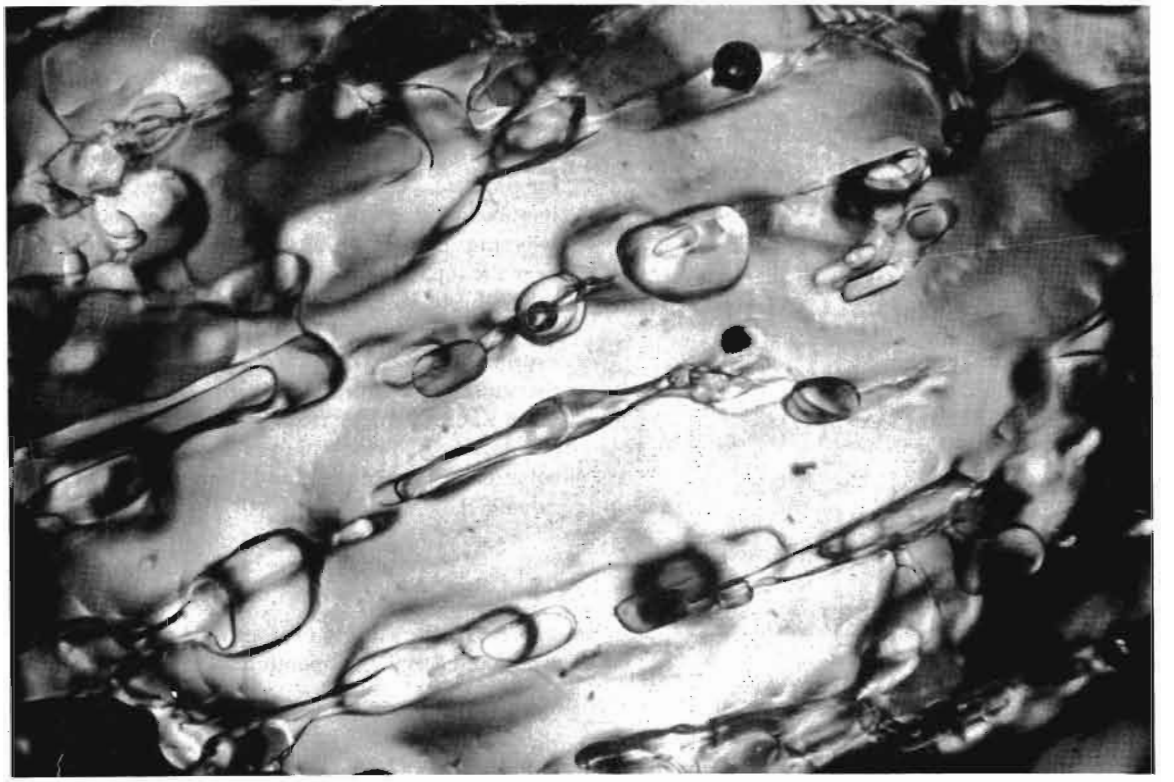

Fig. 3. Photomicrograph of a thin section of sea ice illustrating brine pocket shapes [from *Weeks and Assur,* 1969].

We assume the fields are of the form $E(t) = E_0\, e^{-j\omega t}$ and $E_{2k}(t) = E_{2k_0}\, e^{-j(\omega t+\delta)}$ with no spatial dependence, where $\omega = 2\pi \times 10^8$ rad/s, and δ is the phase difference between the fields. From a polynomial fit of actual arctic sea ice data, we set $\nu_b(l) = 0.29$. We take the following values as the dimensions of a bottom layer inclusion: $b = 0.1$ mm [*Anderson and Weeks,* 1958], $c = 5b = 0.5$ mm [*Kovacs and Morey,* 1978], and $a = 3$ mm [*Weeks and Assur,* 1967]. We evaluate (2) for the two cases of interest, $k = a$ and $k = b$, where $n_a(1) = 9.67 \times 10^{-3}$ and $n_b(1) = 8.39 \times 10^{-1}$.

Case 1: Normal Polarization, $E = E_n$ (parallel to c axis in Figure 2). By using the above parameters

$$\frac{|E_{2b}|}{|E_n|} = 5.26 \times 10^{-3} \tag{3}$$

with $\delta = 85.1°$. This small ratio implies that the electric field is essentially excluded from the brine layer during normal polarization. The exclusion arises physically from the buildup of charge (polarization and free) at the brine/ice interface that creates a large depolarizing field inside the inclusion and terminates the normal field in the ice matrix [*Golden and Ackley,* 1980].

Case 2: Tangential Polarization, $E = E_t$ (perpendicular to c axis in Figure 2). In this case, the moduli of the fields satisfy

$$\frac{|E_{2a}|}{|E_t|} = 4.01 \times 10^{-1} \tag{4}$$

with $\delta = 61.8°$. Now, nearly half the applied field strength has penetrated into the inclusion. This penetration arises physically because the field is directed along the brine/ice interface causing adjacent polarization charges to cancel and free charges to travel rather than accumulate.

Dielectric Behavior

The power flowing from the impinging electromagnetic wave into a brine layer, measured in W/m^3, is given by

$$W = \frac{1}{2} g_2 E_{2k_0}{}^2 \tag{5}$$

where g_2 is the conductivity of brine. Then the ratio of the power losses for the two polarizations is

$$\frac{W_t}{W_n} \approx \frac{(1/2)g_2(4.01 \times 10^{-1})^2 E_0{}^2 V + (1/2)g_1 E_0{}^2 V/\nu_b(1)}{(1/2)g_2(5.26 \times 10^{-3})^2 E_0{}^2 V + (1/2)g_1 E_0{}^2 V/\nu_b(1)} \approx 2200 \tag{6}$$

where we assume that g_1 is the conductivity of pure ice, V is the volume of an ellipsoidal brine layer, and that the amplitude of the wave field in ice is equal to E_0. Thus we expect much more power to be absorbed by bottom sea ice for tangential polarization than for normal polarization. Significant conduction currents are set up in the brine layers during tangential polarization so that there is a large imaginary mixture dielectric constant ($\varepsilon_t'' \propto W_t$) with high attenuation and little signal returned to the receiver. For normal polarization there is a small imaginary mixture dielectric constant ($\varepsilon_n'' \propto W_n$) with significant signal return. Note that we are considering primarily conduction effects, since 100 MHz is below the resonant frequency for water dipole rotations.

In addition to anisotropic absorption of the wave, the asymmetry of the brine inclusions causes anisotropy in the real part of the effective dielectric constant of the sea ice. Horizontal elongation of the brine layers perpendicular to the preferred c axis direction renders the dipole moments of the brine layers larger for tangential polarization than for normal polariza-

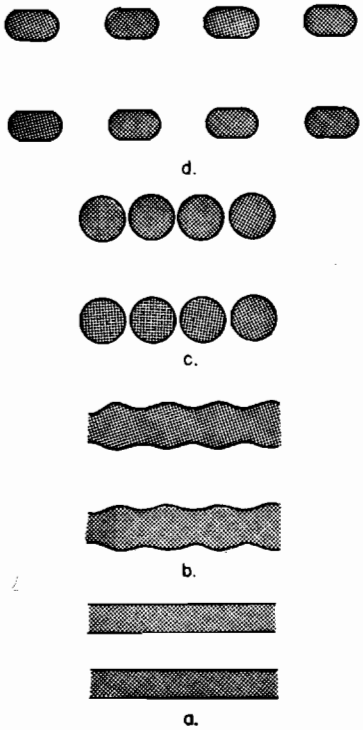

Fig. 4. Brine layers (top view) near the bottom of sea ice (*a*) begin to 'neck' with decreasing temperature further up in the ice sheet(s) and freeze out into cylinders (*c*) and ellipitical cylinders (*d*) [from *Anderson and Weeks,* 1958].

tion. Thus, the real part of the dielectric constant of oriented sea ice is higher for tangential polarization than for normal polarization [*Golden and Ackley,* 1980].

3. Numerical Model

To illustrate how the above effects determine the nature of the reflective anisotropy, we calculate power reflection coefficients (power received from a given interface/incident power) for each of the $n = l + 1$ interfaces of the air/ice/sea water system, and for each polarization.

Layer Dielectric Constants

The effective complex dielectric constant of layer i when subjected to an initially uniform electric field directed along the k axes of the ellipsoids is [*Tinga et al.,* 1973]

$$\varepsilon_k(i) = \varepsilon_1 + \frac{\nu_b(i)\varepsilon_1(\varepsilon_2 - \varepsilon_1)}{n_k(i)(1 - \nu_b(i))(\varepsilon_2 - \varepsilon_1) + \varepsilon_1} \tag{7}$$

The formula is evaluated by using the appropriate values of ε_1 and ε_2, already quoted. (See *Vant* [1976] for a discussion of the applicability of (7) to time varying fields.) The brine volume and depolarization factors are varied for each layer to account for the change in the physical properties of the sea ice with depth.

Immediately above the ice/water interface, the ice is relatively warm and contains a high concentration of elongated brine layers (Figure 4*a*). Further up the temperature decreases and, consequently, the brine layers begin to 'neck' (Figure 4*b*) and change into rows of closely spaced cylinders (Figure 4*c*) and finally into elliptical cylinders (Figure 4*d*) [*Anderson and Weeks,* 1958]. Above the transition zone the brine structure tends to have a more random orientation. To simulate the necking and subsequent freezing-out of the brine layers, we linearly decrease the a/b and c/b ratios from $a:b:c = 30:1:5$ in the bottom layer to $a:b:c = 1:1:0.5$ in the top layer. The vertical dimension c is decreased to a value less than $a = b$ at the top to indicate that the longer dimensions of brine inclusions there have a tendency to be horizontal, due to freezing processes. The model we use is a rough, first-order approximation designed to reflect only the gross features of brine structure: marked anisotropy near the bottom and isotropy near the top.

The brine volume $\nu_b(i)$ is varied according to polynomial fits of data calculated from salinity and temperature profiles obtained from arctic fast ice by W. F. Weeks and A. J. Gow (personal communication, 1978). Data are considered from Cape Krusenstern, Barrow (Chukchi Sea), and Harrison Bay (Figures 5–7). Brine volumes were calculated by using the equation of Frankenstein and Garner [given in *Weeks and Assur,* 1967],

$$\nu_b(i) = \frac{S_i}{10^3}\left[\frac{-49.185}{\theta_i} + 0.532\right] \tag{8}$$

where S_i is the salinity of layer i expressed in parts per thousands, and θ_i is the temperature of layer i expressed in degrees Celsius.

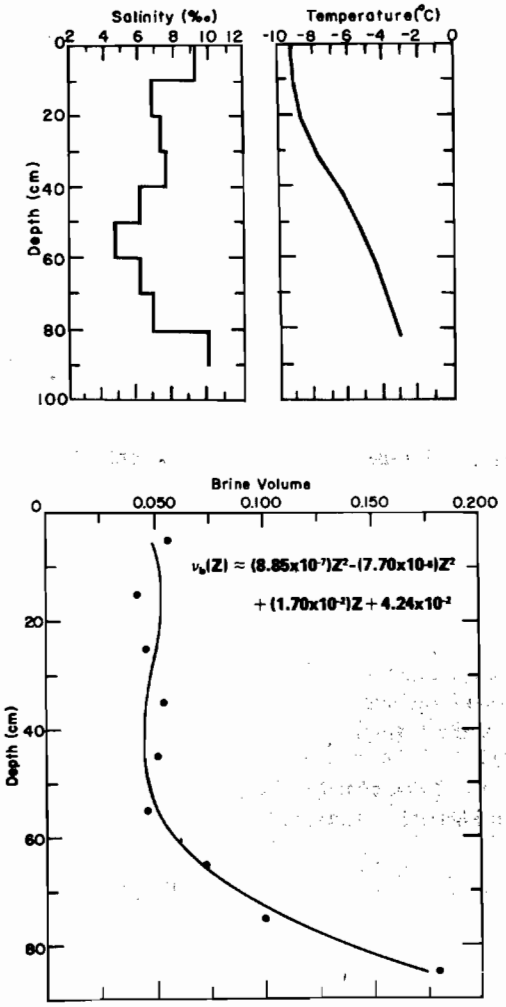

Fig. 5. Temperature, salinity, and brine volume profiles for Cape Krusenstern.

Interfacial Power Reflection Coefficients

We will now calculate interfacial power reflection coefficients $R_k'(i)$ (power reflected by interface i/power incident on interface i) at each interface i for the two polarizations of the incident wave [*Ward*, 1967]. The characteristic bulk impedance $Z_k(i)$ of layer i for polarization along the k axes of the ellipsoids is defined by

$$Z_k(i) = \frac{j\mu_0\omega}{\gamma_k(i)} \tag{9}$$

where $\gamma_k(i)$ is the propagation constant of layer i defined by

$$\gamma_k(i) = \sqrt{\epsilon_0\mu_0\omega^2\epsilon_k'(i) + j\mu_0\omega\, g_k(i)} \tag{10}$$

$g_k(i)$ is the conductivity of layer i for polarization k, and $\mu_0 = 4\pi \times 10^{-7}$ henry/m is the permeability of free space. Since we assume that the losses in sea ice at 100 MHz are primarily due to conduction effects, i.e., $\epsilon_k''(i) = g_k(i)/\epsilon_0\omega$, (11) becomes

$$\gamma_k(i) = \omega\sqrt{\epsilon_0\mu\epsilon_k(i)} \tag{11}$$

The complex amplitude reflection coefficient $r_k(i)$ at an interface i depends on the mismatch of the bulk impedance $Z_k(i-1)$ of layer $i-1$ above the interface and the bulk impedance $Z_k(i)$ of layer i below the interface:

$$r_k(i) = \frac{Z_k(i-1) - Z_k(i)}{Z_k(i-1) + Z_k(i)} \tag{12}$$

On substitution of (10) and (12) this becomes

$$r_k(i) = \frac{\sqrt{\epsilon_k(i)} - \sqrt{\epsilon_k(i-1)}}{\sqrt{\epsilon_k(i)} + \sqrt{\epsilon_k(i-1)}} \tag{13}$$

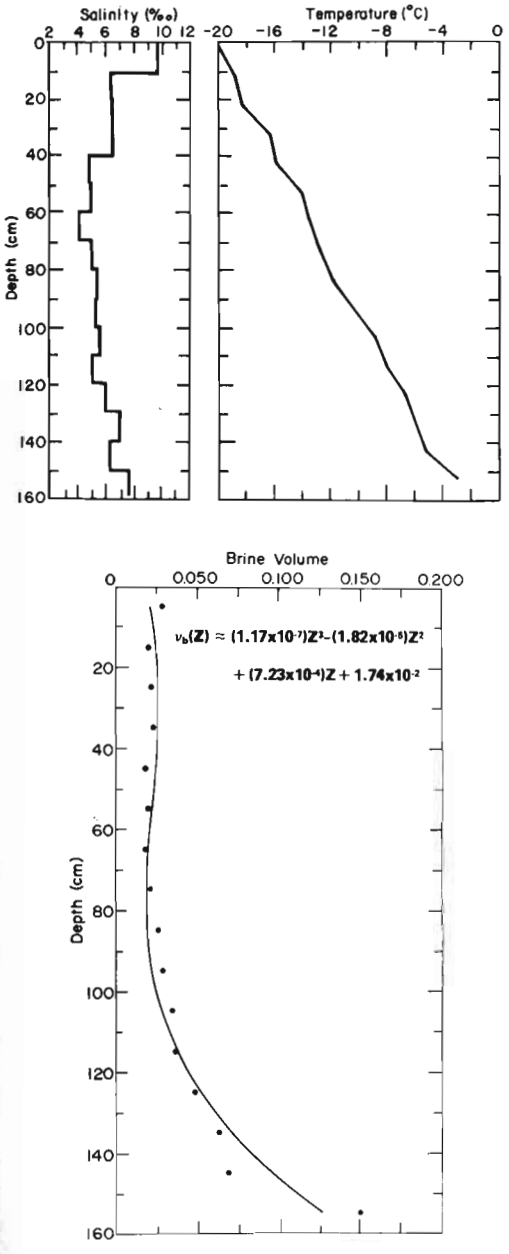

Fig. 6. Temperature, salinity and brine volume profiles for Barrow (Chukchi Sea).

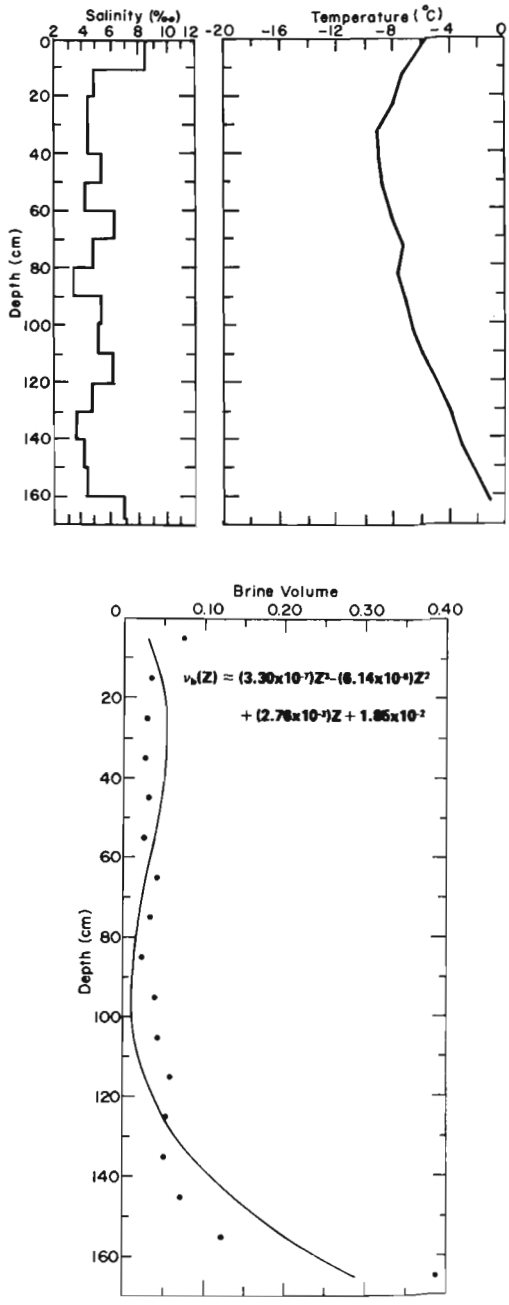

Fig. 7. Temperature, salinity, and brine volume profiles for Harrison Bay.

The interfacial power reflection coefficient $R_k^I(i)$ is obtained from the complex amplitude coefficient through

$$R_k^I(i) = r_k(i)^* \, r_k(i) \tag{14}$$

where the asterisk denotes the complex conjugate. Note that this expression depends on frequency only through the dispersive nature of the dielectric constants of the constituents of the system, sea water, ice, brine, and air.

Bulk Power Reflection Coefficients

Suppose our ice sheet consists of one lossless layer of thickness d. Let a plane wave pulse of temporal duration Δt traveling through air be normally incident on interface 1. Further assume that $\Delta t \ll d/V_I$, where V_I is the wave velocity in ice. The primary pulse returned to the air from interface 2 has the following bulk power reflection coefficient (power returned to air by the interface/power incident on ice slab, without attenuation):

$$R^B(2) = [1 - R^I(1)] \times R^I(2) \times [1 - R^I(1)] \tag{15}$$

A secondary pulse reflected back into the air by interface 2 has the bulk power reflection coefficient

$$R^B(2) = [1 - R^I(1)] \times R^I(2) \times R^I(1) \times R^I(2) \times [1 - R^I(1)] \tag{16}$$

There are infinitely many of these reflected pulses. In our model we neglect multiple reflection effects beyond first order and consider only primary reflections, so that the bulk power reflection coefficient of interface m for polarization k is given by

$$R_k^B(m) = \prod_{i=1}^{m-1} (1 - R_k^I(i))^2 R_k^I(m) \tag{17}$$

for $m = 2, 3, \cdots, n$, and

$$R_k^B(m) = R_k^I(m) \tag{18}$$

for $m = 1$. Figure 8 gives a schematic of the situation.

Attenuated Power Reflection Coefficients

The attenuated power reflection coefficient $R_k^A(i)$ for interface i (power returned to air by interface i/power incident on interface i) is calculated from $R_k^B(i)$ by including losses from travel through sea ice. The amplitude of a monochromatic plane wave traveling one way through a lossy layer i of thickness d is decreased by a factor $e^{-\alpha_k(i)d}$, where $\alpha_k(i)$ is defined by *von Hippel* [1954] as

$$\alpha_k(i) = \frac{2\pi}{\lambda_0} \left\{ \frac{\varepsilon_k'(i)}{2} (\sqrt{1 + (\varepsilon_k''(i)/\varepsilon_k'(i))^2} - 1)^{1/2} \right\} \tag{19}$$

where λ is the free space wavelength. One-way power, therefore, decreases by a factor $(e^{-\alpha_k(i)d})^2$, which may be termed a power transmission coefficient for layer i. We define the attenuated power reflection coefficient by

$$R_k^A(m) = \prod_{i=1}^{m-1} e^{-4d\alpha_k(i)} R_k^B(i) \tag{20}$$

for $m = 2, 3, \cdots, n$, and

$$R_k^A(m) = R_k^I(m) \tag{21}$$

for $m = 1$.

Beam Spread

To obtain realistic reflection coefficients, we estimate beam spreading effects with the Friis transmission formula [*Kraus*, 1953], which gives the ratio of the power in the load of a receiving antenna P_r to the power radiated by a transmitting antenna P_t in terms of the distance between the antennas r, the wavelength λ, and the directivities of the transmitting and receiving antenna, D_t and D_r,

$$\frac{P_r}{P_t} = D_r D_t \left(\frac{\lambda}{4\pi r} \right)^2 \tag{22}$$

The directivity can be expressed as

$$D = \frac{4\pi f(\theta, \phi)_{\max}}{\iint f(\theta, \phi) \, d\Omega} \tag{23}$$

where $f(\theta, \phi)$ is the normalized power pattern and $d\Omega$ is a differential element of solid angle. For simplicity we assume that the transmitting/receiving antenna in our study radiates energy uniformly over a cone subtending a total polar angle of 90°. The directivity $D = D_r = D_t$ then becomes

$$D = \frac{4\pi}{\int_0^{2\pi} d\phi \int_0^{\pi/4} \sin\theta \, d\theta} \approx 6.83 \tag{24}$$

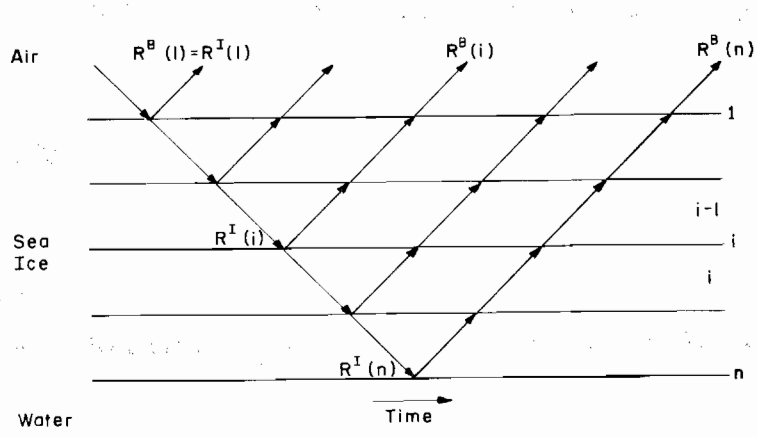

Fig. 8. Schematic diagram for bulk power reflection coefficient calculation [adapted from *Petrin*, 1979].

The final power reflection coefficients $R_k(i)$ are obtained by multiplying each $R_k{}^A(i)$ by the beam spread factor $S(i)$

$$R_k(i) = S(i)\, R_k{}^A(i) \tag{25}$$

where

$$S(i) = \left(\frac{D\lambda}{4\pi \times 2h}\right)^2 \tag{26}$$

and h is the distance from the antenna to interface i. Since reflection measurements are often done with the antenna resting on the ice (but not coupled to the ice), we normalize the $S(i)$ so that $S(1) = 1$. Thus, there is no spreading of the beam for the surface reflection, although it spreads out into the ice.

The above-described numerical method for obtaining reflection profiles was carried out on the computer at Dartmouth College in Hanover, New Hampshire.

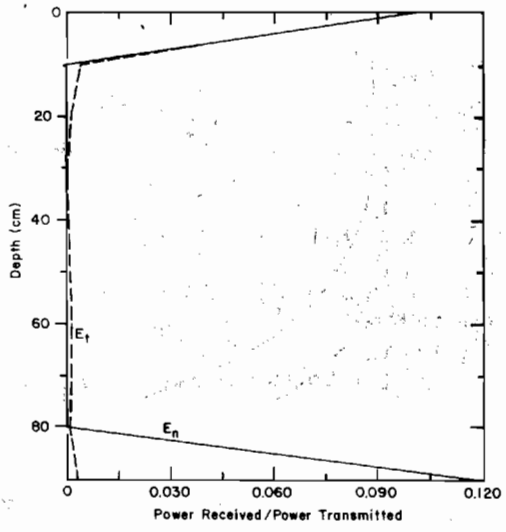

Fig. 9*a*

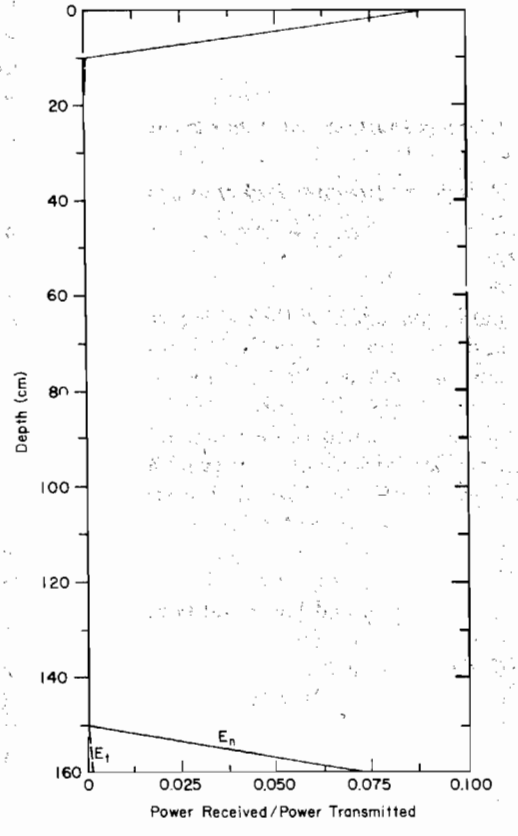

Fig. 9*b*

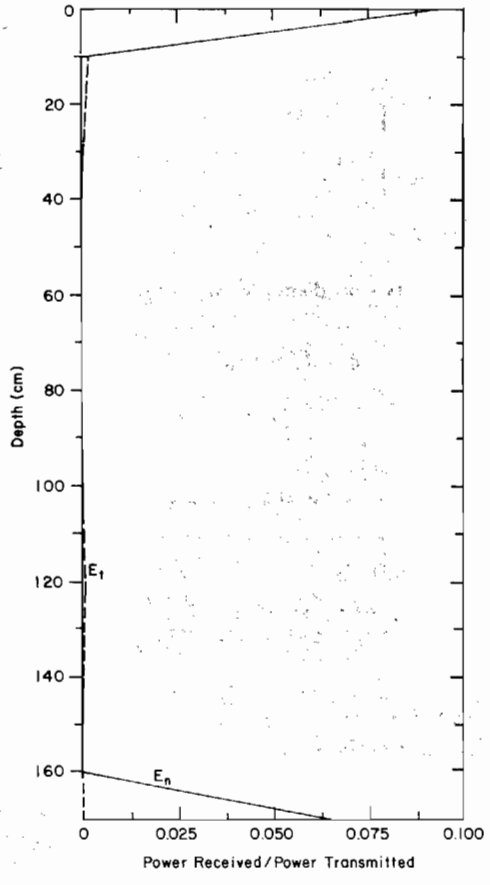

Fig. 9*c*

Fig. 9. Profiles of the $R_k(i)$ for (*a*) Cape Krusenstern, (*b*) Barrow, and (*c*) Harrison Bay. E_t denotes tangential polarization, E_n denotes normal polarization.

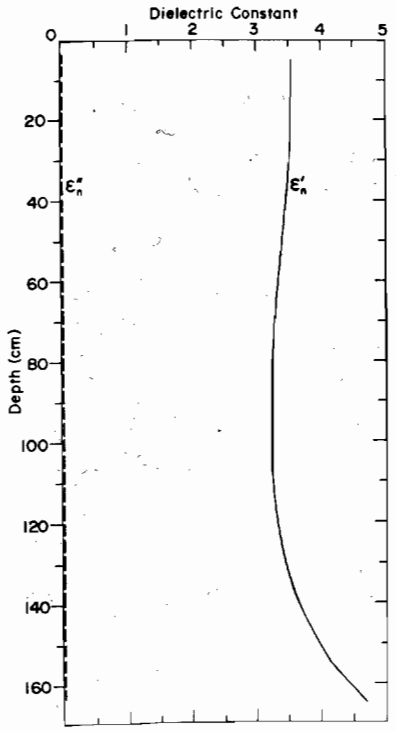

Fig. 10a

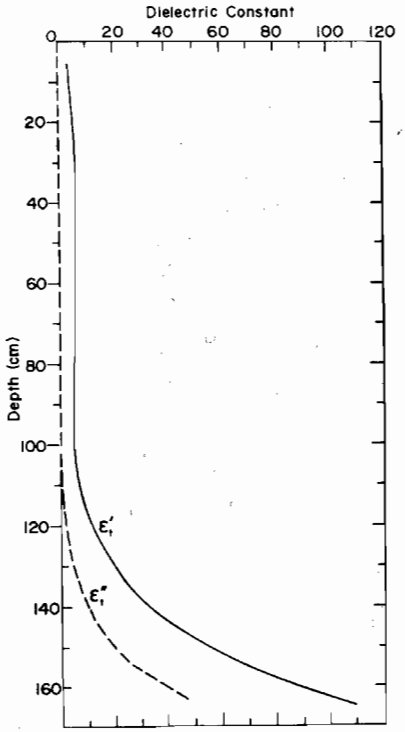

Fig. 10b

Fig. 10. Mixture dielectric constant profiles at Harrison Bay for (*a*) normal polarization and (*b*) tangential polarization.

4. RESULTS

Anisotropic Bottom Reflections

Our model exhibits marked anisotropy of bottom reflections from sea ice at 100 MHz. Figure 9 gives the calculated reflection profiles for the three sites. On the average, about 9% of the transmitted signal is returned to the receiver by the ice/water interface for normal polarization, while the tangentially polarized signal is virtually extinguished ($R_t(n) < 0.003$). Very little, if any, signal is returned from within the ice sheet. Since we have assumed that the top layer is isotropic in the horizontal plane, surface reflections are isotropic.

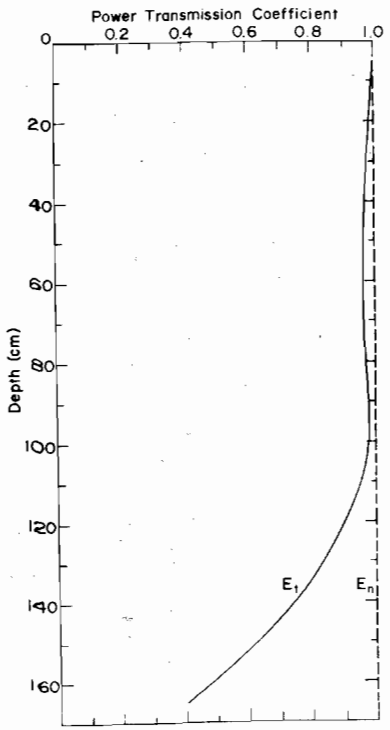

Fig. 11. One-way power transmission coefficient profiles at Harrison Bay. Low transmissions through the layers indicate high attenuation.

Anisotropic Complex Dielectric Constants

In our model, reflective anisotropy can only exist with anisotropic dielectric constants. Figure 10 shows the calculated dielectric constant profiles for Harrison Bay. The anisotropy is most pronounced in the lower regions where the brine volume and a/b ratio are high (i.e., where the brine layers are numerous and well defined). Figure 11 shows the one-way power transmission coefficients $e^{-2d\alpha(i)}$ for Harrison Bay. The wave is highly attenuated in the lower regions during tangential polarization because of the very large contribution of ε'', as suggested previously. The ratio of the imaginary dielectric constants for the bottom layer at Harrison Bay $\varepsilon_t''/\varepsilon_n'' = 47.3/0.027 \approx 1800$ is roughly in agreement with the ratio of the power losses in (6), the calculation of which was based on normal exclusion and tangential penetration of electric flux.

We see from Figure 10*b* that the real part of the mixture dielectric constant of the bottom layer for tangential polarization at Harrison Bay has become quite large (109), in fact larger than that of brine itself (80). The finite extent of the brine layers causes them to behave as macroscopic dipoles. Free and polarization charge can build up at the ends of the brine layers, rendering the sea ice highly polarizable, more so than pure brine with no interfaces.

The combination of the large real and imaginary parts of the mixture dielectric constants for tangential polarization causes the bulk impedance of the bottom sea ice layer to be

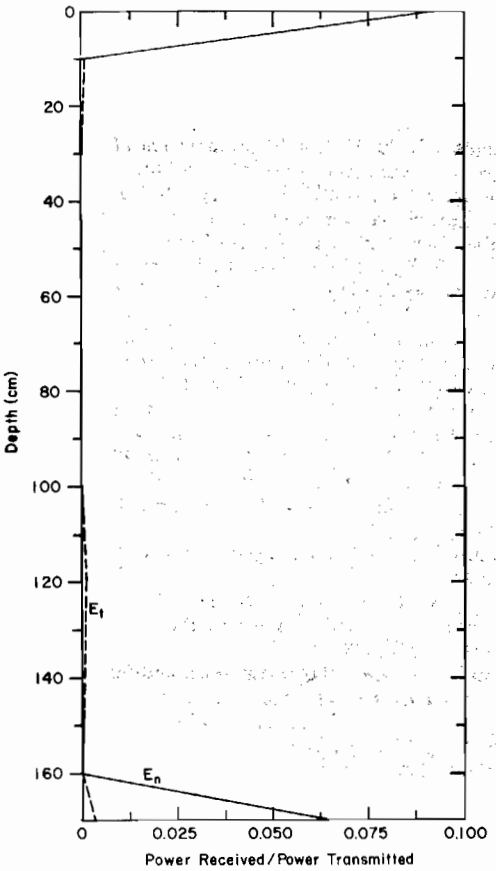

Fig. 12*a*

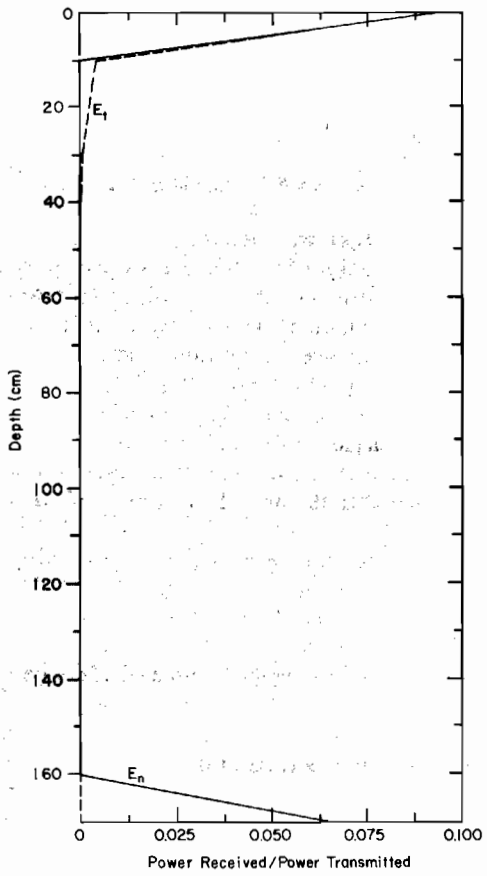

Fig. 12*b*

Fig. 12. Profiles of the $R_k(i)$ at Harrison Bay for (*a*) $a:b:c = 20:1:5$ in the bottom layer and (*b*) $a:b:c = 50:1:5$ in the bottom layer.

similar to that of the water below. Consequently, after downward propagation, the remaining energy of the tangentially polarized wave tends to be transmitted rather than reflected at the ice/water interface. The normally polarized wave encounters a large impedance mismatch and is reflected.

Sensitivity of Parameters

Figure 12 gives reflection profiles for bottom layer brine geometry specified by (1) $a:b:c = 20:1:5$ and (2) $a:b:c = 50:1:5$. A decrease in a allows more effective exclusion of a tangential electric field so that attenuation decreases. An increase in a allows greater penetration of a tangential electric field so that attenuation increases. An increase in c has a similar effect to a decrease in a.

Internal Reflections

It is very interesting to note the appearance of an internal reflection located at a depth of about $2T/3$ for tangential polarization (Figures 9*a*, 9*c*, and 12*a*). In the model this bump in the reflection profile arises from a superposition of two effects. Large brine volume and axial ratio gradients combine to create fairly significant interfacial reflection coefficients which increase with depth. When the ice slab is lossy near the ice/water interface, the bottom reflection coefficients are greatly decreased due to attenuation, leaving a bump higher in the reflection profile. There has been speculation on the existence of this bump in explaining apparent travel-time isotropy [*Kovacs and Morey,* 1979]. We leave this aspect of the reflective anisotropy open to more exhaustive experimentation.

5. DISCUSSION

We have assumed extreme order in the microstructure of sea ice. Effective axial ratios and orientations of brine inclusions at a given depth or region within the sea ice are actually distributed about some mean. However, the standard deviations from preferred bottom c axis azimuth given by *Weeks and Gow* [1979] are between 5° and 15°, indicating a relatively high degree of ordering. Our purpose was to show that if one views brine inclusions as finite, anisotropic conducting bodies that are small compared to wavelength, then the observed reflective anisotropy follows naturally from the behavior of the electromagnetic field around and in the bodies. To illustrate better mechanisms determining reflective anisotropy, we have taken a very simplified model of sea ice. Examination of these limiting cases may render the observed data more understandable.

For instance, our analysis focused on a limiting case of brine structure, namely brine layers (Figures 4*a* and 4*b*). Throughout much of the ice sheet, however, brine structure takes the form of vertical cigar-shaped inclusions (Figures 4*c* and 4*d*). Nevertheless, there will still be anisotropy in electric

flux penetration, as long as the distance between adjacent inclusions is less than the distance between adjacent rows of inclusions. The reflective anisotropy associated with these ordered 'cigars' is weaker than that associated with brine layers.

6. CONCLUSIONS

The reflective anisotropy observed in sea ice can be explained by consideration of the geometrical asymmetries inherent in the brine structure of sea ice with a high azimuthal order of c axis orientation. Anisotropic electric flux penetration into the brine layers determines anisotropy in attenuation of the wave. Axial ratios of 30:1:5 for brine layers in the bottom layer of sea ice give a reasonable level of power returned to the ice surface in the direction normal to the brine layers (parallel to the c axis) while significantly attenuating the power tangential to the brine layers (perpendicular to the c axis).

Variation of brine volume and geometry profiles during model calculations was found to change substantially the reflection profiles. If further experimental work relating observed reflection profiles to sea ice microstructure were done, radar sounding of sea ice could be used as a nondestructive 'spectroscopic' tool giving information on the microstructure variations that ultimately control the strength and other important properties of sea ice. At present, microstructure information can only be obtained by coring a small sample of ice. A methodology such as radar sounding that could extend microstructure information to line profile and area measurements would be valuable in future scientific and engineering investigations of sea ice.

Acknowledgments. The authors would like to thank Wilford Weeks for supplying salinity and temperature data and for reviewing the manuscript, Anthony Gow for supplying data and general information on sea ice structure, and Steven Arcone for review of the manuscript and consultations on electromagnetic wave propagation. This research was sponsored by National Science Foundation grant DPP-77-24528 and this support is also gratefully acknowledged.

REFERENCES

Anderson, D. L., and W. F. Weeks, A theoretical analysis of sea ice strength, *Eos Trans. AGU*, 39, 632–640, 1958.

Campbell, K. J., and A. S. Orange, The electrical anisotropy of sea ice in the horizontal plane, *J. Geophys. Res., 79,* 5059–5063, 1974.

Cherepanov, N. V., Spatial arrangement of sea ice crystal structure, Probl. Arktiki Antarktiki, *38,* 137–140, 1971.

Golden, K. M., and S. F. Ackley, Modeling of anisotropic electromagnetic reflection from sea ice, *Rep. 80-23,* Cold Reg. Res. and Eng. Lab., U.S. Army Corps of Eng., Hanover, N. H., 1980.

Johari, G. P., and P. A. Charette, The permittivity and attenuation in polycrystalline and single-crystal ice Ih at 35 and 60 MHz, *J. Glaciol., 14,* 293–303, 1975.

Kovacs, A., and R. M. Morey, Radar anisotropy of sea ice due to preferred azimuthal orientation of the horizontal c-axes of ice crystals, *J. Geophys. Res., 83,* 6037–6046, 1978.

Kovacs, A., and R. M. Morey, Anisotropic properties of sea ice in the 50-150 MHz range, *J. Geophys. Res., 84,* 5749–5759, 1979.

Kraus, J. P., *Electromagnetics,* McGraw-Hill, New York, 1953.

Petrin, M. F., A computer model of radar echo sounding of multilayer stratified media, Master's thesis, Univ. of New Hampshire, Durham, 1979.

Stratton, J. A., *Electromagnetic Theory,* McGraw-Hill, New York, 1941.

Tinga, W. R., W. A. G. Voss, and D. F. Blossey, Generalized approach to multiphase dielectric mixture theory, *J. Appl. Phys., 44,* 3897–3902, 1973.

Vant, M. R., A combined empirical and theoretical study of the dielectric properties of sea ice over the frequency range 100 MHz to 40 GHz, Ph.D. thesis, Carleton Univ., Ottawa, 1976.

von Hippel, A. R., *Dielectrics and Waves,* MIT Press, Cambridge, Mass., 1954.

Ward, S. H., Electromagnetic theory for geophysical applications in *Mining Geophysics,* Society of Exploration Geophysicists, Tulsa, Okla. 1967.

Weeks, W. F., and A. Assur, *The Mechanical Properties of Sea Ice, CRREL Monogr.,* II-C3, AD, Cold Reg. Res. and Eng. Lab., U.S. Army Corps of Eng., Hanover, N. H., 1967.

Weeks, W. F., and A. Assur, Fracture of lake and sea ice, *Res. Rep. 269,* Cold Reg. Res. and Eng. Lab., U.S. Army Corps of Eng., Hanover, N. H., 1969.

Weeks, W. F., and A. J. Gow, Crystal alignments in the fast ice of arctic Alaska, *Rep. 79-22* Cold Reg. Res. and Eng. Lab., U.S. Army Corps of Eng., Hanover, N. H., 1979.

(Received January 12, 1981;
accepted April 27, 1981.)